

# Modeling and Noise Analysis of a Microcantilever-based Mass Sensor

David M. Harcombe<sup>1</sup>, Michael G. Ruppert<sup>1</sup> and Andrew J. Fleming<sup>1</sup>

**Abstract**—Nanomechanical devices have the potential for practical applications as mass sensors. In microcantilever-based sensing, resonance frequency shifts are tracked by a phase-locked loop (PLL) in-order to monitor mass adsorption. A major challenge in minimizing the mass detection limit comes from the noise present in the system due to thermal, sensor and oscillator noise. There is numerical difficulty in simulating PLLs, as both low frequency phase estimates and high frequency mixing products need to be captured resulting in a stiff problem. By using linear system-theoretic modeling an in-depth analysis of the system is able to be conducted overcoming this issue. This provides insight into individual noise source propagation, dominant noise sources and possible ways to reduce their effects. The developed model is verified in simulation against the non-linear PLL, with each achieving low picogram sensitivity for a 100 Hz loop bandwidth and realistically modeled noise sources.

## I. INTRODUCTION

Microsensing technology is integral to various fields of science and engineering. One such area is the implementation of micromechanical and electromechanical resonators as ultrasensitive transducers [1]. These include microcantilevers, flexural plates, quartz crystal microbalances and surface acoustic wave devices [2]. In recent years, microcantilever-based sensing technology has been used to address challenges in chemical [3] and biological sensing [4] including the detection of volatile organic compounds [5] and gases.

To act as a sensor the cantilever must be coated with a reagent that adsorbs selected molecules to its surface. This process is known as functionalizing the cantilever. The functionalizing site itself is typically a metal layer (such as gold or aluminum) evaporated onto the cantilever [6]. Cantilever functionalization techniques include inkjet printing [7], spray coating [8], spin coating [9] and solution dipping [10]. The first chemical sensing device of this kind was first realized by measuring the static bending of a microcantilever caused by surface stress from molecules adhering to its surface [11].

Resonance frequency changes are induced by either mass loading [12] or changes in the cantilever spring constant [13], which is detected by tracking the resonance frequency. The equation relating the change in mass due to molecule adsorption  $\Delta m$  to the shift in resonance frequency is described by [12]

$$\Delta m = \frac{k}{4\pi^2 n} \left( \frac{1}{f_{\text{res}_1}^2} - \frac{1}{f_{\text{res}_2}^2} \right), \quad (1)$$

\*This work was supported by Ampcontrol.

<sup>1</sup>David M. Harcombe, Michael G. Ruppert and Andrew J. Fleming are with the School of Electrical Engineering and Computing, The University of Newcastle, Callaghan, NSW 2308, Australia. David.Harcombe@uon.edu.au, Michael.Ruppert@newcastle.edu.au and Andrew.Fleming@newcastle.edu.au.

where  $k$  denotes the spring constant of the cantilever,  $n$  is a geometrical constant ( $n = 0.24$  for rectangular cantilevers) and  $f_{\text{res}_1}$  and  $f_{\text{res}_2}$  denote the resonance frequencies before and after the frequency shift respectively. Since the resonance frequency equation involves both mass and stiffness

$$f_{\text{res}} = \frac{1}{2\pi} \sqrt{\frac{k}{m}}, \quad (2)$$

in-order to reduce crosstalk between these properties the sensing layer should be concentrated at the free end of the cantilever [6]. Other factors which cause resonance frequency shifts include adsorption-induced variation in the spring constant [14] and drifting of ambient conditions such as humidity and temperature [15]. To alleviate these issues and increase selectivity, cantilever arrays can be used - achievable with microscale sensing without excessive additional size, cost and power.

To date the majority of microcantilever-based mass sensing uses the optical beam deflection method [16]. However, this requires additional sensor equipment and exact alignment which impose challenges in terms of the overall size, accuracy and repeatability. By employing self-sensing piezoelectric cantilevers [17], [18], these issues can be alleviated. Recent developments into piezoelectric patch placement optimization show that previous limitations such as actuator/sensor feedthrough have been heavily mitigated [19].

## II. MODELING AND ANALYSIS

### A. Non-Linear Phase-Locked Loop

1) *System Description:* The block diagram of the non-linear mass sensing PLL with thermal, sensor and oscillator noise is shown in Fig. 1. As the resonance frequency changes with mass adsorption in real-time, it will be related to the difference between the initial voltage controlled oscillator (VCO) bias frequency  $\omega_{\text{bias}}$  and the loop filter output  $u_\omega$ . Mass sensing is then achieved by relating this measurement to equation (1). The microcantilever is modeled as a transfer function relating an input force to an output displacement

$$G(s) = \frac{\alpha \omega_0^2}{s^2 + \frac{\omega_0}{Q} s + \omega_0^2}, \quad (3)$$

where  $\alpha = 1/k$  [m/N] is the DC-gain of the system,  $Q$  is the quality factor and  $\omega_0$  is the fundamental resonance frequency.

The non-linear nature of a PLL requires biasing around a stable operating point. For this PLL system,  $\omega_{\text{bias}} \approx \omega_0$  to ensure a phase-lock state will be achieved when the system starts. The frequency range in which a PLL will lock is typically limited by the overall loop bandwidth, hence this bias is made as close as possible [20].

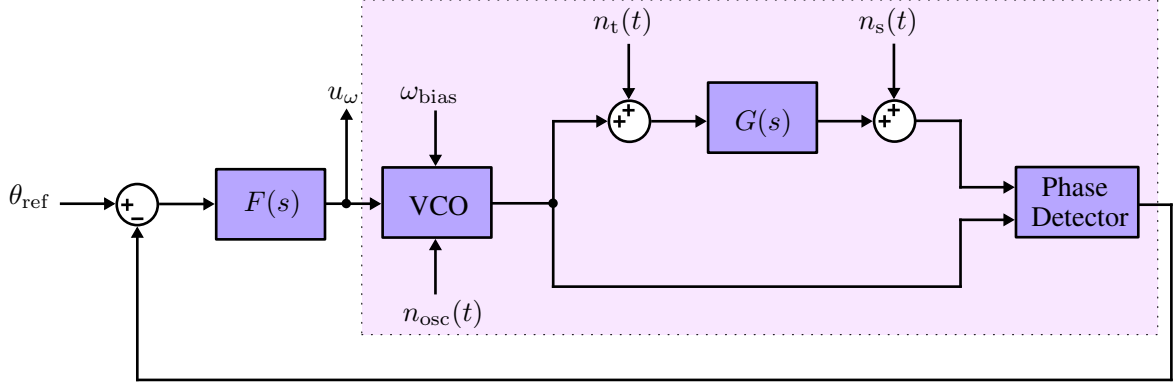


Fig. 1. The non-linear PLL system for microcantilever-based mass sensing with additive white Gaussian thermal noise  $n_t(t)$  and sensor noise  $n_s(t)$ , as well as  $1/f^2$  oscillator noise  $n_{\text{osc}}(t)$ .

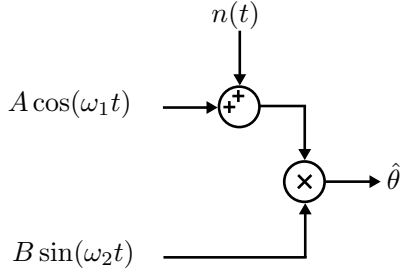


Fig. 2. Diagram of a noise process  $n(t)$  propagating through the phase detector.

Since the VCO produces a sinewave at the fundamental resonance frequency, the output of (3) undergoes a  $-90^\circ$  phase shift. As the two input signals to the phase detector are constantly  $90^\circ$  apart, tracking the resonance frequency of the microcantilever requires  $\theta_{\text{ref}} = 0$ . The loop filter  $F(s)$  provides error regulation and attenuates the high-frequency mixing products at  $2\omega_0$ . For certain applications,  $F(s)$  can be extended to higher orders however more complex stability conditions will need to be found [20].

2) *Non-Linearities*: Non-linearities in the PLL system are introduced through the  $\sin(\cdot)$  function in the VCO and multiplication within the phase detector. According to the sine small-angle approximation,  $\sin(\theta) \approx \theta$  when  $\theta \ll 1$ . This approximation is valid to such a degree it can be taken as absolute during steady-state [21], [20].

A multiplication operation occurs during the typical implementation of a phase detector. If an additive white Gaussian noise is added during the multiplication step, as shown in Fig. 2, then the output phase estimate  $\hat{\theta}$  is described by

$$\hat{\theta} = \underbrace{\frac{AB}{2} \sin(2\omega t)}_{\text{Mixing product}} + \underbrace{\frac{AB}{2} (\omega_1 - \omega_2)t}_{\text{Phase estimate}} + \underbrace{n(t) \cdot A \cos(\omega_2 t)}_{\text{Transposed } n(t)}. \quad (4)$$

The non-linear operation of multiplying  $n(t)$  by a sinusoid results in scaling of the noise density by  $1/\sqrt{2}$  [22]. For both non-linear operations discussed, a whitening of the spectrum is also going to occur [23].

## B. Noise Sources in Microcantilever-based Mass Sensing

1) *Cantilever Thermal Noise*: The theoretical resolution limit of a vibrating cantilever is most prominently limited by thermal noise in the cantilever oscillation signal [24]. This limit is given by the equipartition theorem, which states that if a system is in thermal equilibrium, then the total energy of each vibrational mode (potential plus kinetic energy) has a mean value equal to  $1/2k_B T$ , where  $k_B$  is the Boltzman constant and  $T$  the absolute temperature [25]:

$$\frac{1}{2} k_i \langle x_i \rangle^2 = \frac{1}{2} k_B T. \quad (5)$$

Here,  $x_i$  is the displacement of the  $i$ -th mode of the cantilever and  $k_i$  is the modal stiffness. As with the optical beam deflection sensor, the thermal noise vibrations of the first mode (variance of the cantilever deflections  $\sigma_t$ ) when observed by a piezoelectric sensor are given by [26], [18]

$$\sigma_t^2 = 0.8175 \frac{k_B T}{k}. \quad (6)$$

The variance and the thermal deflection noise spectral density  $N_t(f)$  in [m/Hz] are related by [27]

$$\sigma_t^2 = \int_0^\infty N_t^2(f) df = \int_0^\infty N_f^2 |G(j2\pi f)|^2 df, \quad (7)$$

where  $N_f$  is the thermal white force noise density [28] and  $G(j2\pi f)$  is the cantilever transfer function (3). Solving the integral for the first mode using (6), the thermal deflection noise spectral density is obtained as [18], [28]

$$N_t(f) = \sqrt{0.8175 \frac{2k_B T}{k\pi f_0 Q} \frac{1}{(1 - \frac{f^2}{f_0^2})^2 + \frac{f^2}{f_0^2 Q^2}}}. \quad (8)$$

2) *Sensor Noise*: Traditionally, microcantilever-based mass sensing has used the optical beam deflection (OBD) method [16] to measure the cantilever vibrations, as shown in Fig. 3(a). The sensor noise induced when using an optical source can be described by a Lorentzian peak with a power spectral density of [29]

$$N_{s,\text{OBD}}(f) = \sqrt{\frac{2P_d^2}{\Delta f}}. \quad (9)$$

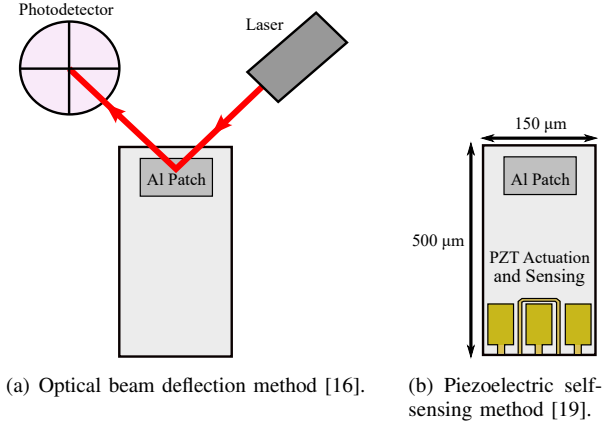


Fig. 3. Microcantilever beam deflection sensing methods.

Here  $P_d$  is the optical power received by the photodetector and  $\Delta f$  is the bandwidth of the photodetector. This spectral density function is flat irrespective of the incident carrier frequency  $\omega$  [29]. For commercial OBD systems, the measurement noise has a white noise spectral density in the range of 100 – 1000 fm/ $\sqrt{\text{Hz}}$  [30], however it requires exact alignment which poses additional challenges in terms of the overall sensor size, accuracy and repeatability. By employing self-sensing piezoelectric cantilevers [17], [18], [19], these issues can be alleviated.

A schematic layout of a cantilever with integrated piezoelectric actuators and sensors is shown in Fig. 3(b). A guard trace prevents actuator sensor feedthrough between the piezoelectric transducers.

The noise spectral density of a piezoelectric read-out scheme is mostly dominated by noise from electronic components within the piezoelectric charge amplifier and was experimentally determined as  $N_{s,PZT}(f) = 700 \text{ fm}/\sqrt{\text{Hz}}$  [18]. From here onwards,  $N_{s,PZT}(f)$  will be simply referred to as  $N_s(f)$ .

While the method does not compare to the lowest noise optical read-out systems to date, there is on-going research into improvement. In particular, the piezoelectric deflection sensitivity could be increased in-order to scale down the electrical noise floor [18].

3) *Oscillator Noise*: The simplest abstraction of an oscillator is an RLC circuit, whose non-ideal resistance adds white thermal noise to the system according to the Johnson-Nyquist model [31]. Leeson's model [32] is an empirical expression built on this concept with several additional features. It describes the normalized single-sideband (SSB) noise spectral density of an oscillator as

$$L(\Delta\omega) = 10 \log \left[ \frac{2Fk_B T}{P_c} \left\{ 1 + \left( \frac{\omega_0}{2Q\Delta\omega} \right)^2 \right\} \left( 1 + \frac{\Delta\omega_{1/f^3}}{\Delta\omega} \right) \right], \quad (10)$$

where  $P_c$  is the carrier signal power,  $F$  is an amplification fitting parameter,  $Q$  is the oscillator quality factor and  $\Delta\omega_{1/f^3}$  dictates the switch from flicker frequency ( $1/f^3$ ) to flicker phase noise ( $1/f^2$ ). With respect to a simple RLC

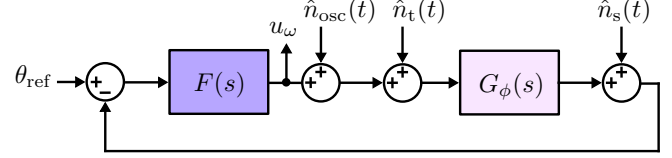


Fig. 4. Linear approximation of microcantilever-based mass sensing PLL. The pink block diagrams represent changes from the non-linear PLL model.

model, there is an additional thermal noise floor dictated by  $2Fk_B T/P_c$  as  $\Delta\omega \rightarrow \infty$  and a  $1/f^3$  factor ( $\Delta\omega_{1/f^3}$ ) for very high  $Q$  oscillators.

Leeson's model (10) predicts that phase noise reduces with increasing carrier power and  $Q$  factor. However, the empirical amplification factor  $F$  has no precise analytical definition and quite often an increased  $Q$  incidentally leads to an increased  $F$  depending on the oscillator circuit [33].

In practice, extremely small offset  $\Delta\omega$  values in the phase noise are considered flat around the carrier [34]. Given this, a numerical approximation to generate oscillator noise is to pass white noise through a band-pass filter [35]

$$H(s) = \frac{(s/z_1 + 1)}{(s/p_1 + 1)}. \quad (11)$$

$z_1 \ll 1$  is chosen to create a purely  $1/f^2$  roll-off in the bandwidth of interest and  $p_1$  must be significantly larger than the carrier frequency as this dictates when the thermal noise floor begins. This gives the oscillator noise spectral density as

$$N_{\text{osc}}(f) = A_{\text{osc}} |H(j2\pi f)|, \quad (12)$$

where  $A_{\text{osc}}$  is an amplification fitting parameter similar to  $F$ . A typical oscillator phase noise specification is between  $-100$  and  $-140$  dBc/Hz at 100 Hz [36].

### C. Linear Approximation

There is numerical difficulty in simulating PLLs, as both low frequency phase estimates and high frequency mixing products at  $2\omega_0$  need to be captured resulting in a stiff system [20]. Fig. 4 shows a linearized model of the non-linear PLL. This model has been developed based on linear approximations so that noise analysis can be conducted using linear-time invariant (LTI) system theory.

1) *Transposed Thermal Noise*: As the cantilever is assumed to be in steady-state with a constant excitation at resonance supplied by the VCO, the thermal phase noise is related to the thermal displacement noise by

$$\int_0^\infty N_f^2 |G(j2\pi f)|^2 df = \int_0^\infty \left( \sqrt{2} \frac{\omega_0}{2Q} N_t(f_0) \right)^2 |G_\phi(j2\pi f)|^2 df. \quad (13)$$

Where the phase dynamics are given by the first order response

$$G_\phi(s) = \frac{2Q}{\omega_0} \times \frac{\frac{\omega_0}{2Q}}{s + \frac{\omega_0}{2Q}}, \quad (14)$$

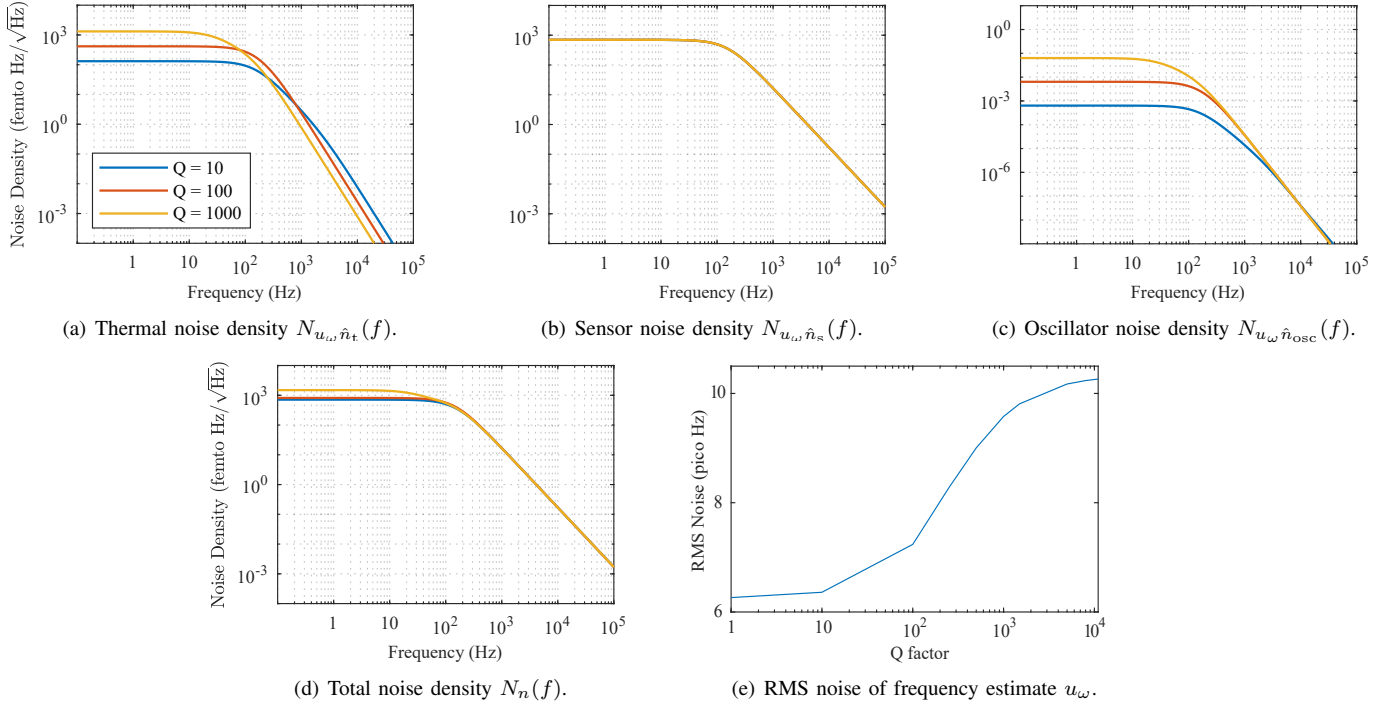


Fig. 5. (a) Thermal noise density, (b) sensor noise density, (c) oscillator noise density, (d) total noise density, and (e) total RMS noise for varying  $Q$  factors and a filter bandwidth of 100 Hz.

here  $2Q/\omega_0$  is the gradient of the phase response of the cantilever system (3) at resonance. Additionally,  $N_t(f_0)$  are the thermal deflections at resonance obtained by evaluating (8) at  $f = f_0$

$$N_t(f_0) = \sqrt{0.8175 \frac{2k_B T Q}{k \pi f_0}}. \quad (15)$$

2) *Transposing VCO Noise*: In the non-linear PLL system shown in Fig. 1, the  $1/f^2$  phase noise directly adds to the argument of the sine function within the VCO [20]. By applying the sine double angle formula, it can be seen that the phase noise will be modulated by  $\cos(\omega_0 t)$ . This is reflected in the linear model by modifying equation (11) to

$$\hat{H}(s) = \frac{1}{2} (H(s + j\omega_0) + H(s - j\omega_0)). \quad (16)$$

3) *Transposing Sensor Noise*: The sensor noise  $n_s(t)$  is additive white Gaussian noise that undergoes modulation by a sinusoidal carrier as seen in Fig. 1. As pure white noise is not physically possible, consider this noise process to have a finite bandwidth in the order of 100 MHz. Due to the difference in speed between the carrier and noise process, the modulated spectrum will appear equivalent in the low bandwidth of interest when comparing  $n_s(t)$  before and after multiplication [37]. However, as this process is the same as that described in equation (4), a scaling of  $1/\sqrt{2}$  needs to be accounted for during the transposing.

#### D. Linear System Noise Analysis

From Fig. 4, the effect of the transposed noise terms  $\hat{n}(t)$  on the frequency output  $u_{\omega}$  can be found by the transfer

functions

$$T_{u_{\omega}, \hat{n}_s}(s) = \frac{U_{\omega}(s)}{\hat{N}_s(s)} = \frac{-F(s)}{1 + F(s)G_2(s)}, \quad (17)$$

$$T_{u_{\omega}, \hat{n}_t}(s) = \frac{U_{\omega}(s)}{\hat{N}_t(s)} = \frac{-F(s)G_2(s)}{1 + F(s)G_2(s)}, \quad (18)$$

and

$$T_{u_{\omega}, \hat{n}_{osc}}(s) = \frac{U_{\omega}(s)}{\hat{N}_{osc}(s)} = \frac{-F(s)G_2(s)}{1 + F(s)G_2(s)}. \quad (19)$$

With knowledge of the sensitivity functions  $T(j2\pi f)$  and noise densities  $N(f)$ , the noise density from each noise source on the frequency estimate can be derived

$$\begin{aligned} N_{u_{\omega}, \hat{n}_s}(f) &= \sqrt{2} N_s(f) |T_{u_{\omega}, \hat{n}_s}(j2\pi f)|, \\ N_{u_{\omega}, \hat{n}_t}(f) &= \sqrt{2} \frac{\omega_0}{2Q} N_t(f_0) |T_{u_{\omega}, \hat{n}_t}(j2\pi f)|, \\ N_{u_{\omega}, \hat{n}_{osc}}(f) &= N_{osc}(f) |T_{u_{\omega}, \hat{n}_{osc}}(j2\pi f)|. \end{aligned} \quad (20)$$

The total noise density on the frequency output is found by

$$N_n(f) = \sqrt{N_{u_{\omega}, \hat{n}_s}(f)^2 + N_{u_{\omega}, \hat{n}_t}(f)^2 + N_{u_{\omega}, \hat{n}_{osc}}(f)^2}, \quad (21)$$

allowing for the standard deviation (RMS value) of the total noise appearing on the frequency estimate to be found by [38]

$$\sigma_n = \sqrt{\int_0^{\infty} N_n(f)^2 df}. \quad (22)$$

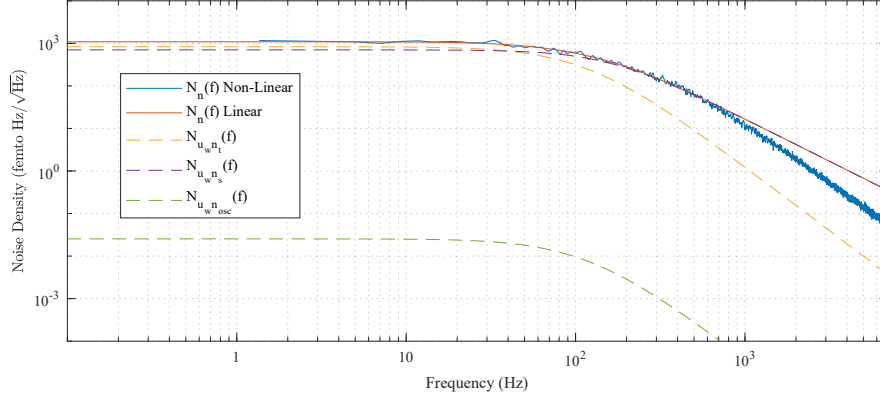


Fig. 6. Comparison of total noise densities of the frequency estimate for the non-linear and linear mass sensing PLL with a loop filter bandwidth of 100 Hz. The simulation parameters are detailed in Section III-A.

In general, it is recommended to evaluate this integral numerically rather than use standard approximation methods based on the order of the sensitivity functions [38].

### III. SIMULATION

#### A. Simulation Parameters

Simulations were conducted to compare the non-linear PLL in Fig. 1 against the linear system-theoretic model in Fig. 4. These microcantilever-based mass sensor models were simulated to assess their noise performance with additive white Gaussian sensor, thermal and oscillator noise present. The simulation parameters are: sampling rate  $F_s = 5$  MHz, cantilever fundamental resonance frequency  $\omega_0 = 2\pi 50 \times 10^3$  rad/s, stiffness  $k = 49$  N/m,  $Q = 400$  and  $F(s)$  is a 2nd-order RC filter.

The sensor noise density is chosen as  $\hat{N}_s(f) = 700$  fm/ $\sqrt{\text{Hz}}$ , while the thermal noise density is  $\hat{N}_t(f_0) = 830$  fm/ $\sqrt{\text{Hz}}$  by evaluating equation (16). The phase noise is shaped to be  $1/f^2$  with  $-140$  dBc/Hz at 100 Hz.

#### B. Linear Approximation

The linear model is investigated through simulation under varying system conditions. In doing so, the cantilever  $Q$  factor is varied with a fixed loop filter bandwidth of 100 Hz.

In Fig. 5(a–c), the individual noise densities of the modeled thermal, sensor and oscillator noise are shown. The combination of these individual noise densities can be seen in Fig. 5(d–e) through the total noise density and RMS noise respectively.

In Fig. 5(a), the DC thermal noise of the system can be seen to increase with higher  $Q$  factors, in accordance with equation (16). Although the DC thermal noise is raised, the mechanical bandwidth of the cantilever is reduced as dictated by  $\omega_0/2Q$ . This results in the total integrated noise from the thermal noise being equal regardless of  $Q$ , as dictated by the equipartition theorem (6), (7).

However, in Fig. 5(e), instead of the RMS noise remaining constant it initially increases as a function of  $Q$  before converging. This is because low  $Q$  values increase the cantilever bandwidth. When this bandwidth exceeds the loop

filter, the perceived total RMS noise is reduced as it doesn't contain all of the thermal noise entering the system.

#### C. Minimum Mass Detection Limit

Fig. 6 compares the total noise density of the frequency estimate between the non-linear and linear PLL. Additionally, the transfer function of each noise density described by (20) is shown. As expected, the dominating noise contribution comes from the cantilever thermal noise. As the frequency increases, the sensor noise begins to dominate as the thermal noise rolls off. The total integrated noise (RMS) of the non-linear and linear simulations are 9.4 and 8.6 picoHz respectively. By reformulating equation (1), we can write

$$\sigma_{\text{mass}} = \left( \frac{k}{4\pi^2 n} \right) \sigma_f, \quad (23)$$

where  $\sigma$  denotes the RMS value. Based on the simulated frequency resolution, for realistic noise source models there is a theoretical minimum mass detection limit of approximately 50 picograms for a 100 Hz bandwidth system.

### IV. CONCLUSION

A challenge when developing ultra-sensitive microcantilever-based mass sensors is the noise present in the system due to thermal, sensor and oscillator noise. A linear model is developed to analyze these noise processes in terms of how they propagate through the system, which is most dominant and if there are any ways to reduce them. By using a system-theoretic LTI approach, the stiff nature of non-linear PLL simulations involving low and high frequency signals was overcome.

The linear approximation of the mass sensor was investigated for several bandwidths and  $Q$  factors, where it was demonstrated to become increasingly accurate for high  $Q$  and closed-loop bandwidth systems. Here it was found that cantilever thermal noise dominates the mass estimate.

The developed models minimum mass detection limit was compared against the non-linear PLL in simulation. It was verified that both systems could achieve a sensitivity of approximately 50 picograms with a loop bandwidth of 100 Hz and realistically modeled noise sources.

## REFERENCES

- [1] T. Thundat and P. I. O. and R. J. Warmack, "Microcantilever sensors," *Microscale Thermophysical Engineering*, vol. 1, no. 3, pp. 185–199, 1997.
- [2] S. W. Wenzel and R. M. White, "Analytic comparison of the sensitivities of bulkwave, surfacewave, and flexural platewave ultrasonic gravimetric sensors," *Applied Physics Letters*, vol. 54, no. 20, pp. 1976–1978, 1989.
- [3] G. A. Campbell and R. Mutharasan, "Monitoring of the self-assembled monolayer of 1-hexadecanethiol on a gold surface at nanomolar concentration using a piezo-excited millimeter-sized cantilever sensor," *Langmuir*, vol. 21, no. 25, pp. 11 568–11 573, 2005.
- [4] G. A. Campbell, M. B. Medina, and R. Mutharasan, "Detection of staphylococcus enterotoxin b at picogram levels using piezoelectric-excited millimeter-sized cantilever sensors," *Sensors and Actuators B: Chemical*, vol. 126, no. 2, pp. 354 – 360, 2007.
- [5] D. Lange, C. Hagleitner, A. Hierlemann, O. Brand, and H. Baltes, "Complementary metal oxide semiconductor cantilever arrays on a single chip: mass-sensitive detection of volatile organic compounds," *Analytical Chemistry*, vol. 74, no. 13, pp. 3084–3095, 2002.
- [6] R. Raiteri, M. Grattarola, H.-J. Butt, and P. Skldal, "Micromechanical cantilever-based biosensors," *Sensors and Actuators B: Chemical*, vol. 79, no. 2, pp. 115 – 126, 2001.
- [7] A. Bietsch, M. Hegner, H. P. Lang, and C. Gerber, "Inkjet deposition of alkanethiolate monolayers and dna oligonucleotides on gold: evaluation of spot uniformity by wet etching," *Langmuir*, vol. 20, no. 12, pp. 5119–5122, 2004, pMID: 15984277.
- [8] M. Baller, H. Lang, J. Fritz, C. Gerber, J. Gimzewski, U. Drechsler, H. Rothuizen, M. Despont, P. Vettiger, F. Battiston, J. Ramseyer, P. Fornaro, E. Meyer, and H.-J. Gntherodt, "A cantilever array-based artificial nose," *Ultramicroscopy*, vol. 82, no. 1, pp. 1 – 9, 2000.
- [9] T. A. Betts, C. A. Tipple, M. J. Sepaniak, and P. G. Datskos, "Selectivity of chemical sensors based on micro-cantilevers coated with thin polymer films," *Analytica Chimica Acta*, vol. 422, no. 1, pp. 89 – 99, 2000.
- [10] J. Fritz, M. K. Baller, H. P. Lang, T. Strunz, E. Meyer, H.-J. Gntherodt, E. Delamarche, C. Gerber, and J. K. Gimzewski, "Stress at the solidliquid interface of self-assembled monolayers on gold investigated with a nanomechanical sensor," *Langmuir*, vol. 16, no. 25, pp. 9694–9696, 2000.
- [11] J. Gimzewski, C. Gerber, E. Meyer, and R. Schlittler, "Observation of a chemical reaction using a micromechanical sensor," *Chemical Physics Letters*, vol. 217, no. 5, pp. 589 – 594, 1994.
- [12] T. Thundat, R. J. Warmack, G. Y. Chen, and D. P. Allison, "Thermal and ambient-induced deflections of scanning force microscope cantilevers," *Applied Physics Letters*, vol. 64, no. 21, pp. 2894–2896, 1994.
- [13] G. Y. Chen, T. Thundat, E. A. Wachter, and R. J. Warmack, "Adsorption-induced surface stress and its effects on resonance frequency of microcantilevers," *Journal of Applied Physics*, vol. 77, no. 8, pp. 3618–3622, 1995.
- [14] S. Cherian and T. Thundat, "Determination of adsorption-induced variation in the spring constant of a microcantilever," *Applied Physics Letters*, vol. 80, no. 12, pp. 2219–2221, 2002.
- [15] H. Lang, M. Baller, R. Berger, C. Gerber, J. Gimzewski, F. Battiston, P. Fornaro, J. Ramseyer, E. Meyer, and H. Gntherodt, "An artificial nose based on a micromechanical cantilever array," *Analytica Chimica Acta*, vol. 393, no. 1, pp. 59 – 65, 1999.
- [16] G. Meyer and N. M. Amer, "Novel optical approach to atomic force microscopy," *Applied Physics Letters*, vol. 53, no. 12, pp. 1045–1047, 1988.
- [17] M. G. Ruppert and S. O. R. Moheimani, "A novel self-sensing technique for tapping-mode atomic force microscopy," *Review of Scientific Instruments*, vol. 84, no. 12, p. 125006, 2013.
- [18] M. G. Ruppert, S. I. Moore, M. Zawierta, A. J. Fleming, G. Putrino, and Y. K. Yong, "Multimodal atomic force microscopy with optimized higher eigenmode sensitivity using on-chip piezoelectric actuation and sensing," *Nanotechnology*, vol. 30, no. 8, p. 085503, jan 2019.
- [19] M. G. Ruppert and Y. K. Yong, "Note: Guaranteed collocated multimode control of an atomic force microscope cantilever using on-chip piezoelectric actuation and sensing," *Review of Scientific Instruments*, vol. 88, no. 086109, 2017.
- [20] D. Abramovitch, "Phase-locked loops: a control centric tutorial," in *Proceedings of the 2002 American Control Conference (IEEE Cat. No. CH37301)*, vol. 1, May 2002, pp. 1–15 vol.1.
- [21] R. Larson and B. Edwards, *Calculus of a Single Variable: Early Transcendental Functions*. Cengage Learning, 2015.
- [22] S. Haykin, *Communication Systems*, 5th ed. Wiley Publishing, 2009.
- [23] G. Wise, A. Traganitis, and J. Thomas, "The effect of a memoryless nonlinearity on the spectrum of a random process," *IEEE Trans. Inf. Theor.*, vol. 23, no. 1, pp. 84–89, Sep. 2006.
- [24] Y. Gan, "Atomic and subnanometer resolution in ambient conditions by atomic force microscopy," *Surface Science Reports*, vol. 64, no. 3, pp. 99 – 121, 2009.
- [25] J. L. Hutter and J. Bechhoefer, "Calibration of atomic force microscope tips," *Review of Scientific Instruments*, vol. 64, no. 7, pp. 1868–1873, 1993.
- [26] H. J. Butt and M. Jaschke, "Calculation of thermal noise in atomic force microscopy," *Nanotechnology*, vol. 6, no. 1, pp. 1–7, jan 1995.
- [27] T. R. Albrecht, P. Grttr, D. Horne, and D. Rugar, "Frequency modulation detection using highq cantilevers for enhanced force microscope sensitivity," *Journal of Applied Physics*, vol. 69, no. 2, pp. 668–673, 1991.
- [28] C. V. Heer, *Statistical mechanics, kinetic theory, and stochastic processes*. New York: Academic, 1972.
- [29] A. García-Valenzuela and J. Villatoro, "Noise in optical measurements of cantilever deflections," *Journal of Applied Physics*, vol. 84, no. 1, pp. 58–63, 1998.
- [30] T. Fukuma and M. Kimura, "Development of low noise cantilever deflection sensor for multienvironment frequency-modulation atomic force microscopy," *Review of Scientific Instruments*, vol. 76, no. 053704, 2005.
- [31] H. Nyquist, "Thermal agitation of electric charge in conductors," *Phys. Rev.*, vol. 32, pp. 110–113, Jul 1928.
- [32] D. B. Leeson, "A simple model of feedback oscillator noise spectrum," *Proceedings of the IEEE*, vol. 54, no. 2, pp. 329–330, Feb 1966.
- [33] T. H. Lee and A. Hajimiri, "Oscillator phase noise: a tutorial," *IEEE Journal of Solid-State Circuits*, vol. 35, no. 3, pp. 326–336, March 2000.
- [34] W. A. Edson, "Noise in oscillators," *Proceedings of the IRE*, vol. 48, no. 8, pp. 1454–1466, Aug 1960.
- [35] D. B. Leeson, "Oscillator phase noise: A 50-year review," *IEEE Transactions on Ultrasonics, Ferroelectrics, and Frequency Control*, vol. 63, no. 8, pp. 1208–1225, Aug 2016.
- [36] A. Hajimiri and T. H. Lee, "A general theory of phase noise in electrical oscillators," *IEEE Journal of Solid-State Circuits*, vol. 33, no. 2, pp. 179–194, Feb 1998.
- [37] R. G. Brown and P. Y. Hwang, *Introduction to Random Signals and Applied Kalman Filtering*, 3rd ed. John Wiley & Sons, 1985.
- [38] A. Fleming and K. Leang, *Design, Modeling and Control of Nanopositioning Systems*. Springer, 01 2014.